The International Journal of Advanced Manufacturing Technology (2018) 98:2791–2799
https://doi.org/10.1007/s00170-018-2435-6

ORIGINAL ARTICLE

Formation mechanism and characterization of shear band in high-speed cutting Inconel718

ZhaoPeng Hao[1] · RuiRui Cui[1] · YiHang Fan[1]

Received: 21 December 2017 / Accepted: 16 July 2018 / Published online: 25 July 2018

Abstract
Nickel-based alloy Inconel718 is one kind of complex alloy with multiple components. There is complex cutting deformation (shear localization of material) in high-speed cutting process. The chip shows a serrated shape. Through analyzing the chip morphology, the change of microstructure and development of shear band is analyzed, and the formation mechanism of the shear band is revealed. Based on the formation mechanism of shear band, the coupled elastoplastic-damage constitutive model is proposed to describe the shear stress during the cutting process. The shear band width has been determined by micrographic observations and theoretical model calculation. The experimental and theoretical results show that the shear band width in chip formation decreases linearly with an increase in the cutting speed.

Keywords Inconel718 · High-speed cutting · Cutting deformation · Serrated chip · Shear band

1 Introduction

Inconel718 is one kind of nickel-based superalloy. It is widely used in the aviation, aerospace and nuclear industry because of its superior properties such as excellent creep resistance, less harmful phase, high-temperature oxidation resistance, excellent high-temperature strength, good thermal stability, and thermal fatigue resistance [1, 2]. Inconel 718 is precipitation strengthened by a body-centered tetragonal γ'' phase and face-centered cubic γ'. There existed complicated cutting deformation. The chip shows a serrated shape, which resulted in instability of cutting process [3–5]. They have been the focus concern of academic and business.

An important aspect of the high-speed machining Inconel718 is formation of shear bands in the process of cutting deformation. Komanduri et al. [6, 7] observed the shear band in chip which was obtained in high-speed cutting Inconel718 experiment. Based on the balance between thermal softening and work hardening, modeling of thermomechanical shear instability was performed to describe the shear localization phenomenon.

Pawade et al. [8] presented an analytical model that predicted specific shearing energy of the Inconel 718 in shear zone. It considered formation of shear bands that occurred at higher cutting speeds during machining, along with the elaborate evaluation of the effect of strain, strain rate, and temperature dependence of the shear flow stress using Johnson–Cook equation. The theoretical and experimental results showed that the shear band spacing in chip formation increases linearly with an increase in the feed rate.

Shockey et al. [9] carried out the tests of tubular Hopkinson torsion bar specimens. The evolution of shear bands in Inconel 718 under high-rate shear loading was tracked by high-speed photography. Failure of Inconel 718 occurred by initiation and propagation of mode II cracks.

There are a few studies on the shear band formation and characterization in machining Inconel 718. Most of the research focused on titanium alloys and high-strength steels. Molinari et al. [10] presented an experimental analysis of orthogonal cutting of a Ti6Al4V at different cutting speeds. The shear band width and the distance between bands were determined by micrographic observations, analyzing their dependence upon cutting velocity.

✉ YiHang Fan
fyh1911@126.com

[1] School of Mechatronic Engineering, Changchun University of Technology, Changchun 130012, China

Table 1 Chemical composition and mechanical properties of Inconel718

Material	Chemical composition (wt%)									
	Ni	Cr	Nb	Mo	Ti	C	Si	Mn	B	Fe
Inconel718	51.75	17	5.15	2.93	1.07	0.042	0.21	0.03	0.006	last
	Mechanical properties									
	Yield	Tensile		Toughness	Shrinkage		Elongation		Density	
	σ0.2 (MPa)	σ_b (MPa)		a_k (J/cm^2)	ψ (%)		δ_5 (%)		ρ (kg/m^3)	
	1260	1430		40	40		24		8280	

Burns et al. [11] demonstrated that, by means of a one-dimensional continuum model, the shear stress in machining over the tool-material contact length was not homogeneous. It can lead to repeated oscillations in the plastic flow of the workpiece material during high-speed machining high-strength steels, leading to the repeated formation of adiabatic shear bands.

Perzyna et al. [12] studied the instability phenomena and adiabatic shear band localization in thermoplastic flow processes. It has been proved that the investigation of the instability phenomena and adiabatic shear band localization criteria can be based on an analysis of acceleration waves and particularly on the instantaneous adiabatic acoustic tensor.

In high-speed machining Ti-6Al-4V alloy, Ye et al. [13] proposed a model to describe the periodic adiabatic shear band evolution. The microscopic observations of chips revealed that the transition of chip morphology from continuous to serrated can be attributed to a repeated adiabatic shear band formation, and the shear band could evolve to a higher level as the cutting speed increases. Based on the experimental observations, a theoretical model, taking into account the shear band evolution and material convection, was developed to predict the segment spacing, which agreed with the theory of Meyers et al. [14], Xue et al. [15, 16], and Zhou et al. [17].

According to the previous studies, in this present paper, through analyzing the chip morphology, the change of microstructure and development of shear band is analyzed, and the formation mechanism of the shear band is revealed. Based on the formation mechanism of shear band, the coupled elastoplastic-damage constitutive model is proposed to describe the shear stress during the cutting process. The shear band width is analyzed in terms of the cutting parameters. The analysis is finally validated by performing machining tests on Inconel 718.

2 Experimental procedure

2.1 Workpiece material and cutting tool

The workpiece used in this study was Inconel718 bar (solid solution + aging). The chemical composition and mechanical properties of Inconel718 are shown in Table 1. The indexable carbide turning tools were used in the experiments. The tool information is shown in Table 2.

2.2 Experimental method

In order to study the change of microstructure and development of shear band and the formation mechanism of the shear band, quick-stop tests (the cutting speed v_c is from 80 to 120 m/min) were carried out to obtain the chip root. The cutting depth a_p is 2 mm and the feed rate f is 0.2 mm/r). The quick-stop devices can make the cutting tool separate from the workpiece quickly during the process of cutting and "freeze" the cutting zone when retracting. The metallographic graphs of chips were obtained using metallurgical microscope after polishing and etching the chip root specimen.

3 Results and discussion

3.1 Chip morphology and shear stress

The micrographs by SEM (scanning electron microscope) of chip root are shown in Fig. 1. According to Fig. 2, the chip presented serrated and the deformation is not uniform. A shear band is formed between each sawtooth, and the width of shear band decreases with cutting speeds. The width of the shear band varies with the cutting speed as shown in Fig. 2.

Table 2 Parameters of cutting tool used in experiments

Tool material	Tool shape	Nose radius γ_ε (mm)	Tool rake angle γ_o (°)	Tool relief angle α_o (°)	Side cutting edge angle κ_γ (°)
PVD-TiAlN	SNMG1204	0.4	0	6	90

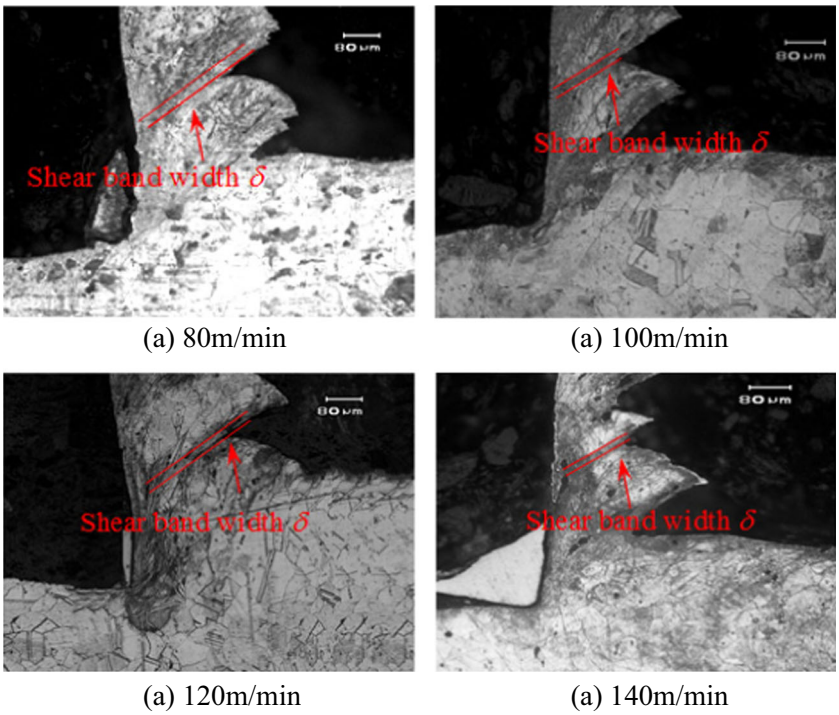

(a) 80m/min (a) 100m/min

(a) 120m/min (a) 140m/min

Fig. 1 Micrographs by SEM of chip root. **a** 80m/min. **b** 100m/min. **c** 120m/min

The shear stress τ in cutting zone can be expressed as [5]:

$$\tau = \frac{F\cos\omega}{b_D h_D/\sin\phi} \quad (1)$$

where τ is shear stress; F is resultant cutting force; ω is the angle between the resultant cutting force and the shear band; ϕ is shear angle when shear band is formed.

Figure 3 shows the variation of shear stress with cutting speeds. According to Fig. 3, with the increase of cutting speed, the shear stress decrease. It can illustrate that the softening of material in cutting zone is more obvious with cutting speeds.

3.2 Formation mechanism of shear band

As the material began to shear along line 1, due to the strain in the bulk of the segment due to upsetting, cracks appeared in the free surface of the cutting layer, as shown in Fig. 4. These fields in the direction of crack were subjected to severe strain in a narrow band between the segments. The stress shock received by materials and high strain rate led to mechanical fragmentation of grains, grain boundary migration, and grain mechanical rotation. These grains broken into tiny subgrain and then became the core of recrystallization and grow up, as shown in Fig. 5. This dynamic recrystallization mechanism is similar to the

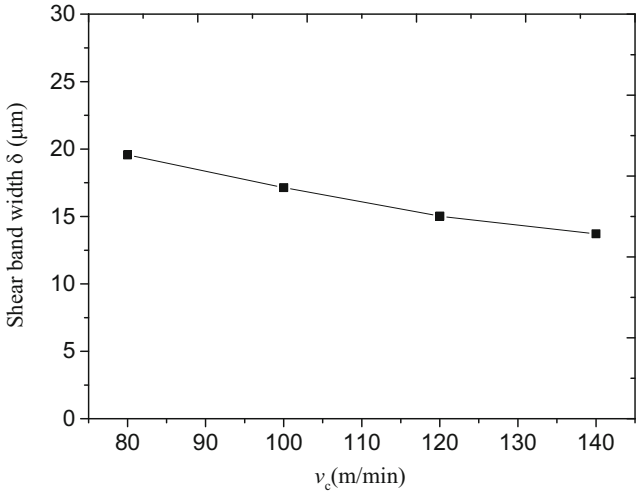

Fig. 2 Variation of width of shear band with cutting speeds

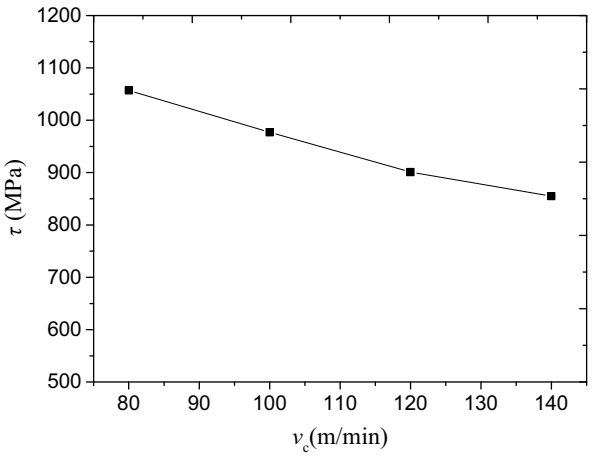

Fig. 3 Variation of shear stress with cutting speeds

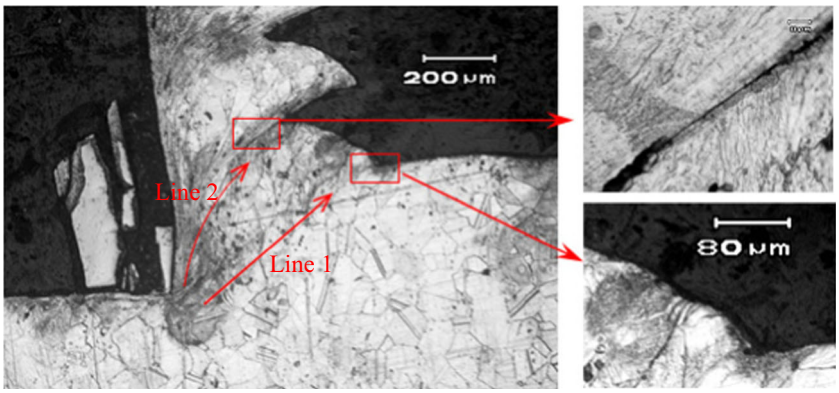

Fig. 4 Micrograph of shear band

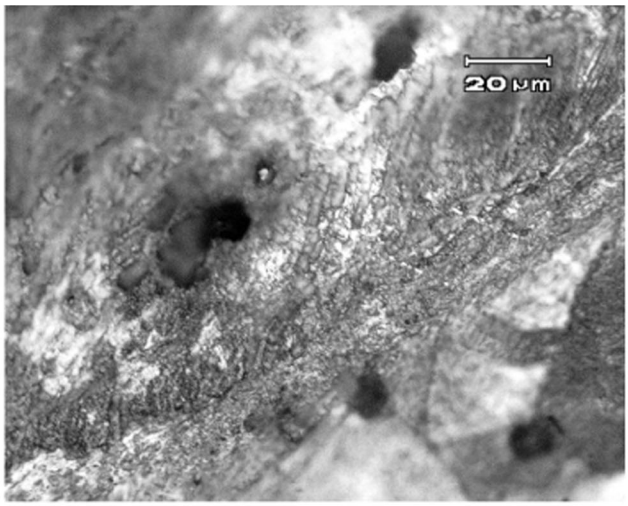

(a) Little deformation of the grains within the segment

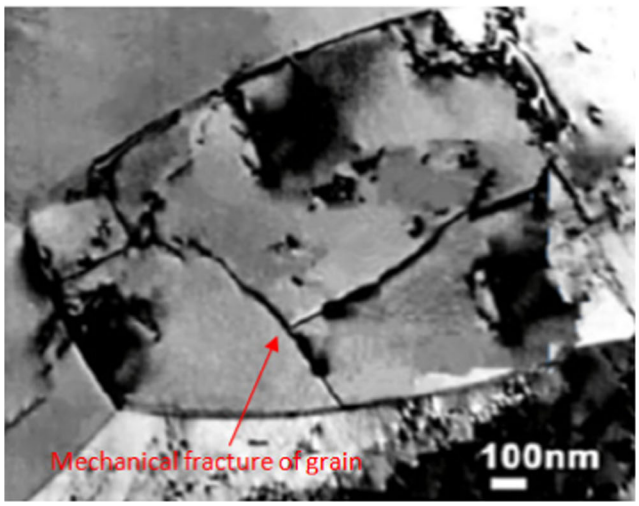

(b) Mechanical fracture of grain

Fig. 5 Micro-morphology of shear band. **a** Little deformation of the grains within the segment. b Mechanical fracture of grain

research conclusion of Hines et al. [18] and Li et al. [19]. The dynamic recrystallization led to thermoplastic instability, which was governed by the thermomechanical response of the work material under the conditions of cutting.

However, the strain in segment was rather small, as can be seen by the very little deformation of the grains within the segment in Fig. 5a. At this moment, in the cutting layer, the freshly wedge sheared (nascent) surface was formed along the line 1. When the tool entered into the wedge cutting layer, the chip segment then moved up the ramp, and a new segment began to form. When the new augment upsetting, wedge sheared (nascent) surface developed into line 2. Shearing between the segments along line 2 ceased when the next localized shear band formed along line 1, and the shear band finally formed.

3.3 Characterization of shear band width

According to the study of adiabatic shear band formation in the process of high-speed cutting Inconel718 by Molinari [10], the shear band width δ can be expressed as

$$\delta = \frac{12\sqrt{2m_s}k_c T_{\text{initial}}}{a\tau v_\tau} \tag{2}$$

where m_s is the strain rate sensitivity; k_c is the heat conductivity; $k_c = 0.0136T + 12.96$; a is the material constant which is dependent on the temperature and strain rate; v_τ is the shear flow resistance; T_{initial} is the initial temperature.

In order to determine these parameters in Eq. (2), compressive SHPB (split Hopkinson pressure bar) test at elevated temperature was suitable to achieve strain rate of the same order in cutting process. The schematic diagram of the SHPB test equipment is shown in Fig. 6. The specimen subjected to different strain rate loading was placed between the incident bar and the transmitter bar. The experimental specimens were heated by high-frequency

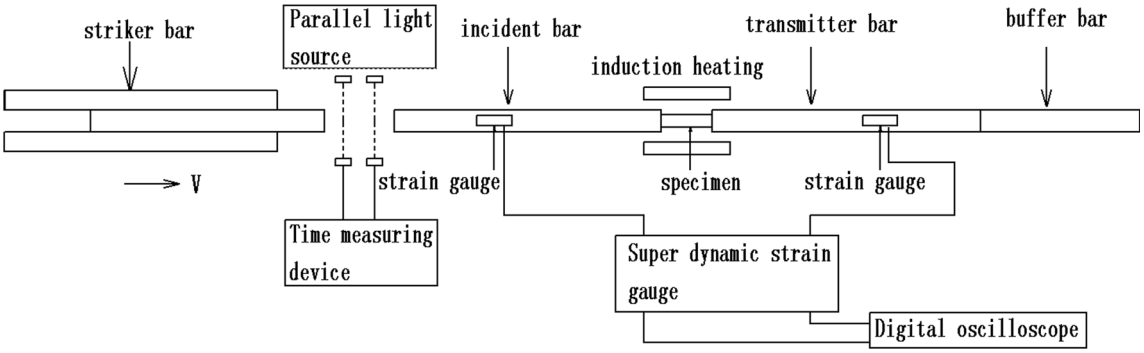

Fig. 6 Schematic diagram of the SHPB test equipment

electromagnetic heating device. SHPB experimental principle is based on one-dimensional elastic assumption and uniformity assumption theory, and ignores the friction and inertia effect.

(1) Determination of m_s, a

The parameter m_s characterizes the tendency of strengthening with the different conditions in plastic deformation of materials. The value of m_s can be obtained from the stress-strain curve of Inconel718 under different conditions. The stress-strain curve (σ-ε) of Inconel718 under different temperatures and strain rates is shown in Fig. 7.

The strain rate sensitivity is defined as

$$m_s = \left| \frac{\partial \ln \sigma_p}{\partial \ln \dot{\varepsilon}} \right| \tag{3}$$

where σ_p is the peak flow stress; $\dot{\varepsilon}$ is the strain rate.

Figure 8 shows the linear relationship curve of $\ln\sigma$-$\ln\dot{\varepsilon}$ at different temperatures and strain rates. We can get the value of m_s ($m_s = 0.2$).

The parameter a reflects the variation of material flow stress with temperature and strain rate. It can be estimated by stress-strain curve at different temperatures and strain rates, which is the slope of relationship curve of $\ln\sigma$-$\ln 1/T$.

$$a = \left| \frac{\partial \ln \sigma_p}{\partial \ln 1/T} \right| \tag{4}$$

Figure 9 illustrates the linear relationship curve of $\ln\sigma$-$\ln 1/T$ at different temperatures and strain rates. We can get the value of a ($a = 0.11$).

(2) Determination of τ

In the light of the formation mechanism of shear band, the shear stress is the result of the interaction of plastic deformation and fracture. The coupled elastoplastic-damage constitutive model of τ can be expressed as

$$\tau = \phi(D)\tau_{JC} \tag{5}$$

For the thermal viscoplastic behavior of workpiece materials, the Johnson–Cook constitutive relation can be used to describe τ_{JC}. It is expressed as

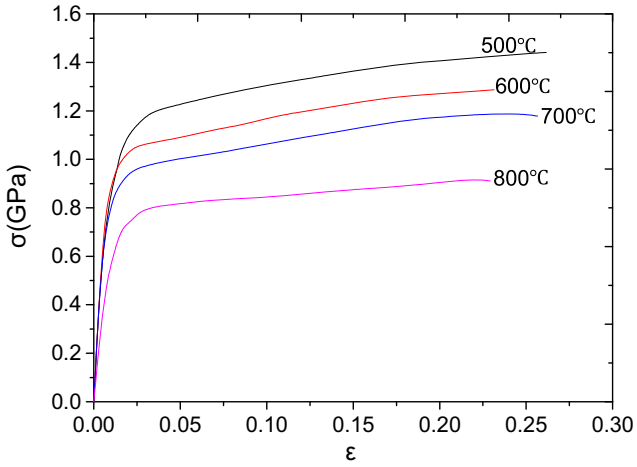

(a) Stress-strain curves under different temperatures

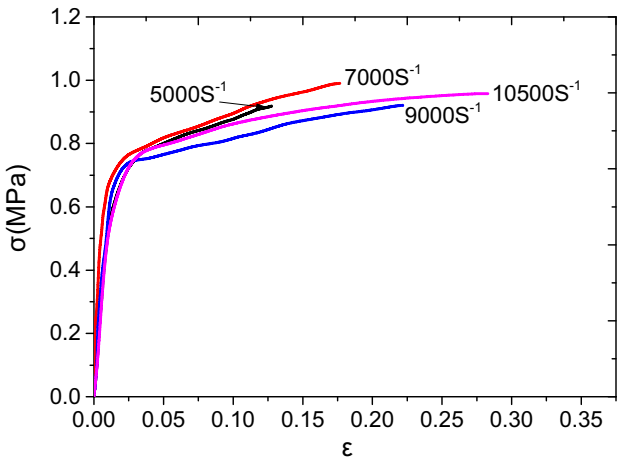

(b) Stress-strain curves under different strain rates

Fig. 7 Stress-strain curves under different conditions. **a** Stress-strain curves under different temperatures. **b** Stress-strain curves under different strain rates

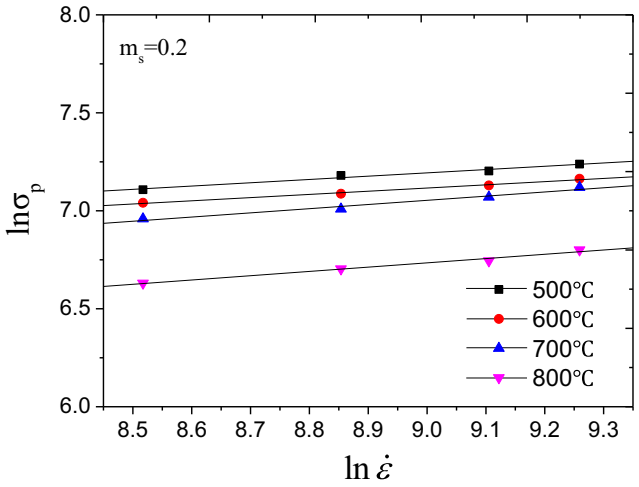

Fig. 8 Relationship curve of $\ln\sigma$-$\ln\dot{\varepsilon}$

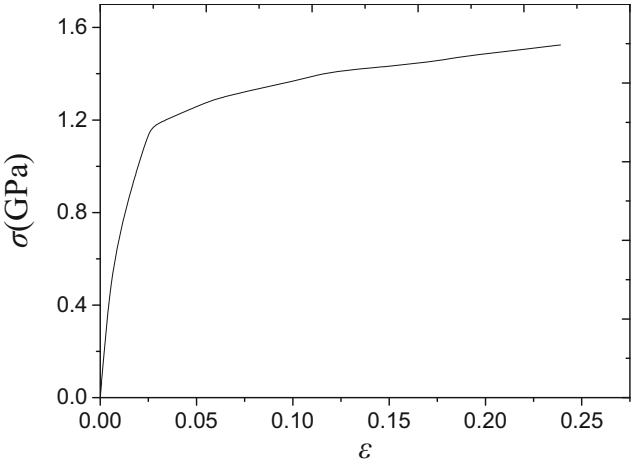

Fig. 10 Stress-strain curves in the quasi-static experiment

$$\tau_{JC} = \frac{1}{\sqrt{3}}\left[A + B\left(\frac{\gamma}{\sqrt{3}}\right)^{n}\right]\left[1 + C\ln\left(\frac{\dot{\gamma}}{\sqrt{3}\dot{\bar{\varepsilon}}}\right)\right]\left[1-\left(\frac{T-T_a}{T_m-T_a}\right)^{m}\right] \tag{6}$$

where A, B, n, C, and m are material constants; γ is shear strain, $\dot{\gamma}$ is shear strain rate, and $\dot{\bar{\varepsilon}}$ is reference strain rate; T is the current temperature and T_a is the room or reference temperature. T_{m} is the melting temperature; m is temperature softening parameter.

The quasi-static compression experiment using electronic universal testing machine was carried out to obtain the stress and strain data at room temperature. The reference strain rate is 0.001 s^{-1} [20], as shown in Fig. 10.

According to Figs. 7 and 10, the parameters A, B, C, m, and n were finally calculated. $A = 985$, $B = 949$, $C = 0.01$, $m = 1.65$, and $n = 0.4$.

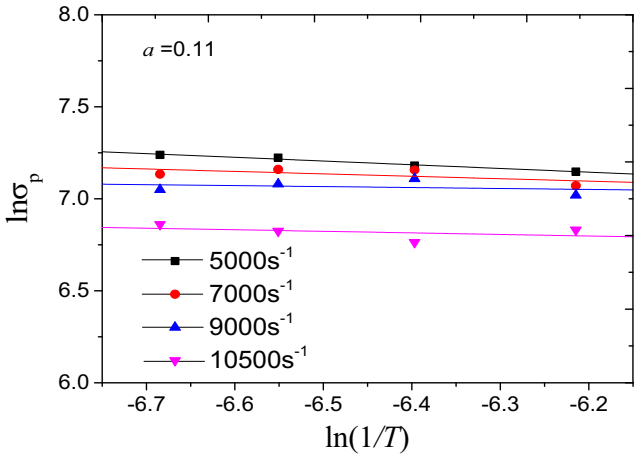

Fig. 9 Relationship curve of $\ln\sigma$-$\ln 1/T$

Due to the generation of cracks and the expansion, the weakening function $\phi(D)$ is proposed and it is expressed as:

$$\phi(D) = 1 - D^{\chi} \tag{7}$$

where D is the damage parameter and χ is a material constant which is changed with temperature and strain rate.

$$\chi = -0.0124T + 0.0014\,\dot{\varepsilon} + 1.0942 \tag{8}$$

The simplest form of a damage accumulation rule is a linear function, which means that the damage is proportional to the equivalent plastic strain. The plastic damage process is characterized in rate form [21].

$$\dot{D} = \frac{\dot{\bar{\varepsilon}}}{\varepsilon_f} \tag{9}$$

For the coupled elastoplastic-damage constitutive model, fracture strain can be expressed as

$$\varepsilon^f = \varepsilon^f_{JC}\mu(\theta) \tag{10}$$

And then the damage variable can be rewritten as

$$\dot{D} = \frac{\dot{\bar{\varepsilon}}}{\varepsilon_f} = \frac{\dot{\bar{\varepsilon}}}{\varepsilon^f_{JC}\mu(\theta)} \tag{11}$$

$$D = \int_0^{\varepsilon_f} \frac{1}{\varepsilon^f_{JC}\mu(\theta)}\Delta\varepsilon \tag{12}$$

where ε^f_{JC} is Johnson–Cook damage strain, $\mu(\theta)$ is the second kind of the Lode angle dependent function.

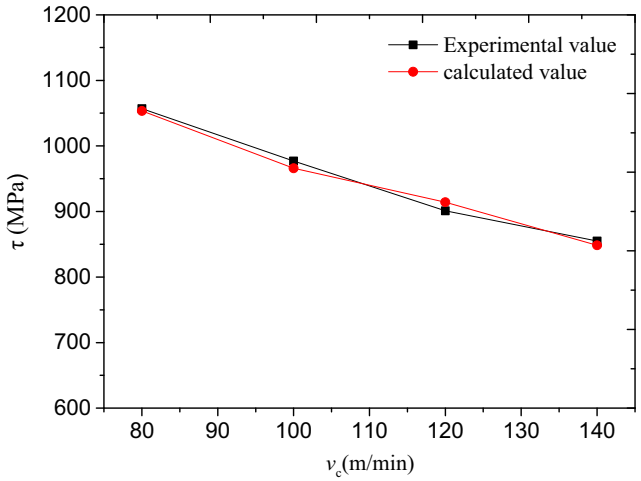

Fig. 11 Comparison between the calculated and experimental values of shear stress τ

ε_{JC}^{f} determines the damage evolution process of materials under different stress, strain rate, and temperature. It can be expressed as

$$\varepsilon_{JC}^{f} = \frac{\gamma_{JC}^{f}}{\sqrt{3}} = [D_1 + D_2\exp(D_3\eta)]\left[1 + D4\ln\left(\dot{\bar{\varepsilon}}/\dot{\bar{\varepsilon}}_0\right)\right][1 + D5(T - T_a/T_m - T_a)] \quad (13)$$

where D_i ($i = 1, 2, 3, 4, 5$) are material constants. The constants of Johnson–Cook damage model were taken from the literature [22] for Inconel718:

$D_1 = 0.04$, $D_2 = 0.75$, $D_3 = -1.45$, $D_4 = 0.04$, $D_5 = 0.89$; η is the stress triaxiality; $\eta = \sigma_H/\overline{\sigma}$; σ_H is the hydrostatic stress; $\overline{\sigma}$ is the equivalent stress.

As pointed out by Gruben et al. [23], the small length–width ratio of the gauge area in the plane strain specimens yields a nearly plane strain stress state. Assuming plane strain state, the equivalent stress in terms of principal stresses is:

$$\overline{\sigma} = \frac{\sqrt{3}}{2}\sigma_1 \quad (14)$$

The hydrostatic pressure σ_H can be described as

$$\sigma_H = \frac{\sigma_1 + \sigma_2 + \sigma_3}{3} = \frac{\sigma_1}{2} \quad (15)$$

and then, $\eta = \frac{\sigma_H}{\overline{\sigma}} = \frac{1}{\sqrt{3}}$.

The second kind of Lode dependence function$\mu(\theta)$ is defined by

$$\mu(\theta) = \beta + (1-\beta)\left(\frac{6|\theta|}{\pi}\right)^k \quad (16)$$

where k is a shape parameter ($k = 1$). The second kind of the Lode dependence function degenerates to a perfect circle, then $\beta = 1.5$ and$\theta = \frac{\pi}{6}$.

The comparison between the calculated and experimental values of shear stress τ is shown in Fig. 11. The error is about 0.925%.

(3) Determination of v_τ

Figure 12 shows a schematic of the velocity about shear band. v_{chip} is the chip velocity relative to the tool, v_c is the cutting speed, ϕ is shear angle ($\phi \approx 45^\circ$), and γ_0 is tool rake angle ($\gamma_0 = 0$). The velocity component is constant ($v_c \sin\phi$) through the thickness of the shear band, due to the incompressibility condition.

According to the velocity vector relationships, the chips flow speed along the rake face of the tool is expressed as

$$v_{\text{chip}} = \frac{v_c \sin\phi}{\cos(\phi - \gamma_0)} \quad (17)$$

In high-speed machining, the shear velocity v_τ can be calculated by

$$v_\tau = \frac{v_c \sin\phi + v_c \sin\phi \tan(\phi - \gamma_0)}{2} \quad (18)$$

Finally, the width of shear band in machining Inconel 718 can be expressed as

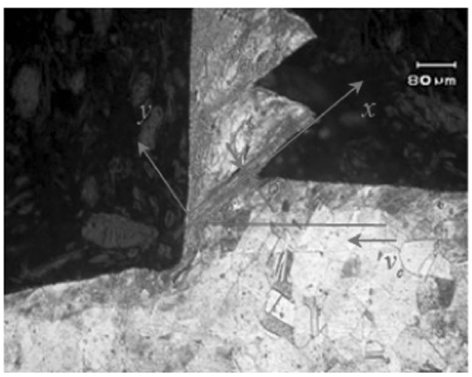

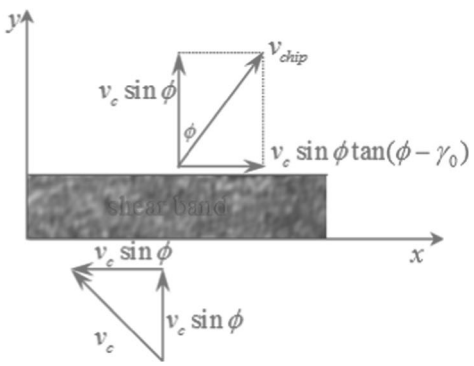

Fig. 12 Schematic of the velocity about shear band

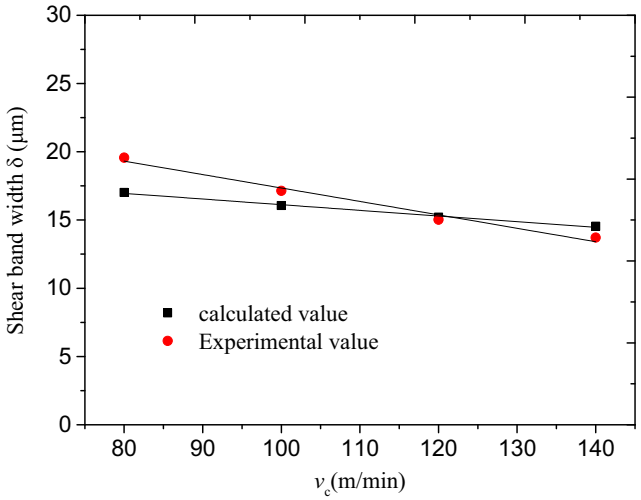

Fig. 13 Comparison between the calculated and experimental values of shear band width

$$\begin{cases} \delta = \dfrac{12\sqrt{2m_s}k_c T_{\text{initial}}}{a\tau v_\tau} \\ m_s = 0.2 \\ a = 0.11 \\ k_c = 0.0136T + 12.96 \\ \tau = \phi(D)\tau_{JC} \\ v_\tau = \dfrac{v_c\sin\phi + v_c\sin\phi\tan(\phi - \gamma_0)}{2} \\ T_{\text{initial}} = \text{Initial temperature} \end{cases} \tag{19}$$

The theoretical value of the shear band width at different cutting speeds is calculated and compared with the experimental value. The comparison results are shown in Fig. 13, with an average error of 6.64%. It can be seen that the theoretical value of the shear band width agrees well with the experimental data, and the shear band width decreases with the increase of cutting speed. The experimental results are consistent with the conclusions which was obtained in the literature [24].

4 Conclusions

Through analyzing the chip morphology, the change of microstructure and development of shear band is analyzed, and the formation mechanism of the shear band is revealed. The conclusions can be drawn as follows:

(1) In machining Inconel 718, mechanical fragmentation of grain occurs when the shear band material received the stress shock and at high strain rate. The grain boundary migration and grain mechanical rotation also occur and then the micro cracks are formed. The dynamic recrystallization occurred, which lead to thermoplastic instability.

(2) Based on the formation mechanism of shear band, a coupled elastoplastic-damage material model is proposed for calculation of shear stress. The model takes into account the Lode angle dependent function in the plastic strain to failure expression of the Johnson–Cook failure criterion.

(3) The shear band width is analyzed in terms of the cutting parameters. The theoretical value of the shear band width at different cutting speeds is calculated and compared with the experimental value. The comparison results show that the theoretical value of the shear band width agrees well with the experimental data, and the shear band width decreases with the increase of cutting speed.

Funding information This work is supported by the National Natural Science Foundation of China: (51505038) and the Science and Technology project of Education Department of Jilin Province (JJKH20170564KJ, JJKH20170562KJ).

References

1. Zhu DH, Zhang XM, Ding H (2013) Tool wear characteristics in machining of nickel-based superalloys. Int J Mach Tool Manu 64: 60–77
2. Fan YH, Hao ZP, Zheng ML, Sun FL, Yang SC (2013) Study of surface quality in machining nickel-based alloy Inconel 718. Int J Adv Manuf Technol 69:2659–2667
3. Venkatesan K, Ramanujam R, Kuppan P (2017) Investigation of machinability characteristics and chip morphology study in laser-assisted machining of Inconel 718. Int J Adv Manuf Technol 91: 3807–3821
4. Costes JP, Guillet Y, Poulachon G, Dessoly M (2007) Tool-life and wear mechanisms of CBN tools in machining of Inconel 718. Int J Mach Tools Manuf 47(7–8):1081–1087
5. Gao D, Hao ZP, Han RD, Chang YL, Muguthu JN (2011) Study of cutting deformation in machining nickel-based alloy Inconel 718. Int J Mach Tool Manu 51(6):520–527
6. Komnaduri R, Schroeder T (1986) On hear instability in machining nickel-iron base superalloy. J Eng Ind 108:93–100
7. Hou ZB, Komanduri R (1997) Modeling of thermo mechanical shear instability in machining. Int J Mech Sci 39(11):1273–1314
8. Pawade RS, Sonawane HA, Joshi SS (2009) An analytical model to predict specific shear energy in high-speed turning of Inconel718. Int J Mach Tool Manu 49(12):979–990
9. Shockey DA, Simons JW, Brown CS, Kobayashi T (2007) Shear failure of Inconel 718 under dynamic loads. Exp Mech 47:723–732
10. Molinari A, Musquar C, Sutter G (2002) Adiabatic shear banding in high speed machining of Ti–6Al–4V: experiments and modeling. Int J Plast 18:443–459
11. Burns TJ, Davies MA (2002) On repeated adiabatic shear band formation during high-speed machining. Int J Plast 18:487–506
12. Perzyna P (1994) Instability phenomena and adiabatic shear band localization in thermoplastic flow processes. Acta Mech 106(3–4): 173–205
13. Ye GG, Xue SF, Jiang MQ, Tong XH, Dai LH (2013) Modeling periodic adiabatic shear band evolution during high speed machining Ti-6Al-4V alloy. Int J Plast 40:39–55

14. Meyers MA, Nesterenko VF, LaSalvia JC, Xue Q (2001) Shear localization in dynamic deformation of materials: microstructural evolution and self-organization. Mater Sci Eng A 317(1–2):204–225
15. Xue Q, Meyers MA, Nesterenko VF (2002) Self-organization of shear bands in titanium and Ti-6Al-4V alloy. Acta Mater 50:575–596
16. Xue Q, Meyers MA, Nesterenko VF (2004) Self organization of shear bands in stainless steel. Mater Sci Eng A 384:35–46
17. Zhou F, Wright TW, Ramesh KT (2006) The formation of multiple adiabatic shear bands. J Mech Phys Solids 54:1376–1400
18. Hines JA, Vecchio KS, Ahzi S (1998) A model for microstructure evolution in adiabatic shear bands. Metall Mater Trans A 29(1): 191–203
19. Li Q, Xu YB, Lai ZH, Shen LT, Bai YL (2000) Dynamic recrystallization induced by plastic deformation at high strain rate in a Monel alloy. Mater Sci Eng A 276:250–256
20. Wang XY, Huang CZ, Zou B, Liu HL, Zhu HT, Wang J (2013) Dynamic behavior and a modified Johnson-Cook constitutive model of Inconel718 at high strain rate and elevated temperature. Mater Sci Eng A 580:385–390
21. Liang X (2007) Damage accumulation and fracture initiation in uncracked ductile solids subject to triaxial loading. Int J Solids Struct 44:5163–5181
22. Erice B, Gálvez F (2014) A coupled elastoplastic-damage constitutive model with Lode angle dependent failure criterion. Int J Solids Struct 51:93–110
23. Gruben G, Fagerholt E, Hopperstad OS, Bovik T (2011) Fracture characteristics of a cold-rolled dual-phase steel. Eur J Mech A Solids 30:204–218
24. Yang QB, Liu ZQ, Shi ZY, Wang B (2014) Analytical modeling of adiabatic shear band spacing for serrated chip in high-speed machining. Int J Adv Manuf Technol 71(9–12):1901–1908